Fiber Stippling: An Illustrative Rendering for Probabilistic Diffusion Tractography

Mathias Goldau*
University of Leipzig and
Max Planck Institute for
Neurological Research Cologne

Alexander Wiebel†
Zuse Institute Berlin

Nico Stephan Gorbach‡
Max Planck Institute for
Neurological Research Cologne

Corina Melzer§
Max Planck Institute for
Neurological Research Cologne

Mario Hlawitschka¶
University of Leipzig

Gerik Scheuermann‖
University of Leipzig

Marc Tittgemeyer**
Max Planck Institute for
Neurological Research Cologne

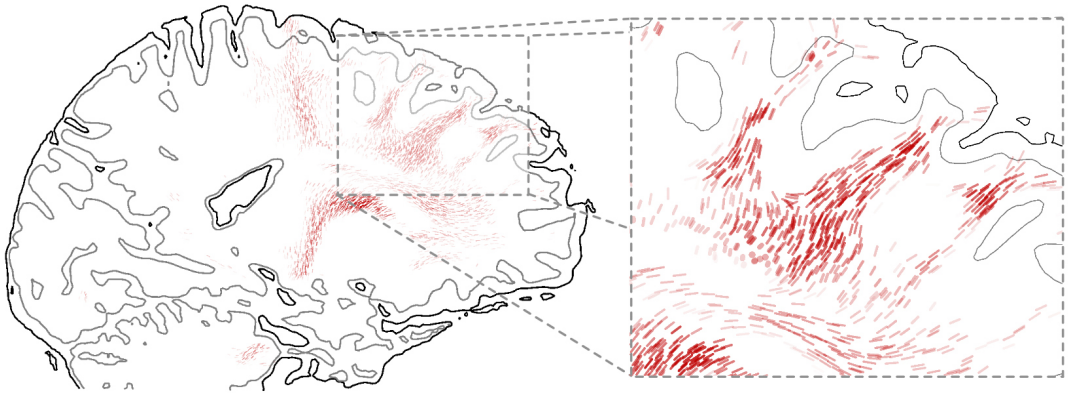

Figure 1: Illustration of an example diffusion tractogram seeded in the anterior prefrontal cortex and probing the connectivity underlying the diffusion tensor field in the human brain. Overview of a whole sagittal slice (left) and close-up (right).

ABSTRACT

One of the most promising avenues for compiling anatomical brain connectivity data arises from diffusion magnetic resonance imaging (dMRI). dMRI provides a rather novel family of medical imaging techniques with broad application in clinical as well as basic neuroscience as it offers an estimate of the brain's fiber structure completely non-invasively and in vivo. A convenient way to reconstruct neuronal fiber pathways and to characterize anatomical connectivity from this data is the computation of diffusion tractograms.

In this paper, we present a novel and effective method for visualizing probabilistic tractograms within their anatomical context. Our illustrative rendering technique, called fiber stippling, is inspired by visualization standards as found in anatomical textbooks. These illustrations typically show slice-based projections of fiber pathways and are typically hand-drawn. Applying the automatized technique to diffusion tractography, we demonstrate its expressiveness and intuitive usability as well as a more objective way to present white-matter structure in the human brain.

Keywords: Scalar Field Data, Tensor Field Data, Illustrative Visualization, DTI, Probabilistic Tractography.

*e-mail: math@informatik.uni-leipzig.de
†e-mail: wiebel@zib.de
‡e-mail: nico.gorbach@nf.mpg.de
§e-mail: corina.melzer@nf.mpg.de
¶e-mail: hlawitschka@informatik.uni-leipzig.de
‖e-mail: scheuermann@informatik.uni-leipzig.de
**e-mail: tittgemeyer@nf.mpg.de

Index Terms: I.3.3 [Computer Graphics]: Picture/Image Generation—Line and curve generation;

1 INTRODUCTION

To date, anatomical connectivity information has been revealed mostly from animal models. These focus on the measurements of axonal degenerating subsequent to lesion, active transport of tracers that are injected while the animal is still alive or, most frequently on post mortem tracer application. The respective techniques require high levels of effort and skill, cannot be applied to an individual living human subject, and are not suited for obtaining an exhaustive connectivity pattern of the whole brain, or even of a certain region in the brain. Furthermore, tract variability is difficult to assess since only a limited set of connections can be traced per specimen.

Illustration of tract tracing usually reveals slice-wise projections of tracer substance arrival and only allows for reconstruction of pathways by means of photo processing software [30], or even –in older anatomical textbooks- hand drawings.

With diffusion MRI (dMRI), a technique has emerged that allows in vivo and non-invasive characterization of long-range axonal connectivity in the brain [19, 18, 14]. This technique probes the direction-dependent mobility of water molecules by measuring dephasing of spins of protons in the presence of a spatially varying magnetic field ('gradient') at a certain time after excitation. As microstructural barriers influence the mobility of the molecules, it is possible to infer certain direction-dependent aspects of the microanatomy, such as fiber directions. This allows the reconstruction of white matter fiber pathways, referred to as diffusion tractography [26, 17, 8, 29], and an estimation of anatomical connectivity. However, noise and artifacts present in the MR scan introduce uncertainty pertaining to fiber direction. Further uncertainty in model parameters is caused by using simple models to describe the com-

plex nature of the diffusion signal [5]. Probabilistic tractography provides a means to quantize the anatomical connectivity pattern in terms of a scalar field of probabilities in order to infer useful information about fiber tract direction while taking the aforementioned uncertainty into account. More precisely, probabilistic tractograms can be regarded as an appropriate approximation to the anatomical connectivity profile representing small individual brain areas (usually small MRI voxels).

To date, different methods have been proposed to perform probabilistic tractography. Among them are the construction of a probabilistic density function proposed by Behrens et al. [5] and a random walk method suggested by Anwander et al. [3]. The latter approach is used in this paper and describes the path taken by a particle starting from a given seed voxel near the gray- and white matter boundary and transitioning through target voxels within the white matter volume based upon local diffusivity measurements (i.e. local diffusivity measurements determine the transition probability from voxels to neighboring voxels). The random walk of a particle starting from the same seed voxel is repeated many times such that the relative frequencies at which particles transitioned to target voxels give an appropriate measure of the probability of connectivity from particular seed voxels to target voxels.

In the following, we give a detailed description of fiber stippling, a novel and effective method for visualizing probabilistic tractograms. The illustration of the tractograms is embedded in an outline of their anatomical context. The rendering technique is inspired by illustrations as can be found in anatomical textbooks, and is based on the metaphor of a slab showing only sections of fiber pathways that lie in the slab. These sections are represented as line stipples. In particular, the main contributions of this paper are

- a new illustrative technique to render probabilistic tractography data employing a widely accepted metaphor,
- an integration of this technique with a gray matter/white matter context and
- a publicly available implementation of the integrated technique in an open-source framework for medical and brain data visualization (http://www.OpenWalnut.org).

2 Related Work

This section is divided into two parts. In the first part we will describe illustration techniques - as usually applied in modern anatomical textbooks - we will be doing this at the example of the book of Schmahmann and Pandya [30] as this has become quasi-standard to reference fiber pathways in the (macaque) brain. In the second part we present a brief overview of previous work on visualizing probabilistic tracts.

2.1 Inspiration from anatomical textbook

In 2006, Schmahmann and Pandya published an anatomical textbook on fiber pathways from the cerebral cortex of macaque monkey brains [30]. For constructing the illustrations for the book, they employed microscopy with radioactive tracers. This is not suited for in vivo analysis, but it allows for a great level of detail, almost an order of magnitude beyond the resolution that might be achievable by current dMRI-based methods.

Their findings of connections in the brain are presented slice-wise; each carefully selected slice depict tracts with hand-drawn points and dashes indicating their directionality as well as anatomical context with the help of white matter and gray matter boundary lines as shown in Figure 2. The method we present in this paper mimic the tracts using line stipples and the boundaries with isolines of structural MRI data such as T1-weighted MR images. Still there is a huge difference of precision between both methods, but the increase in precision of dMRI scanners is expected to continue. This will make in vivo measurements of a comparable precision feasible.

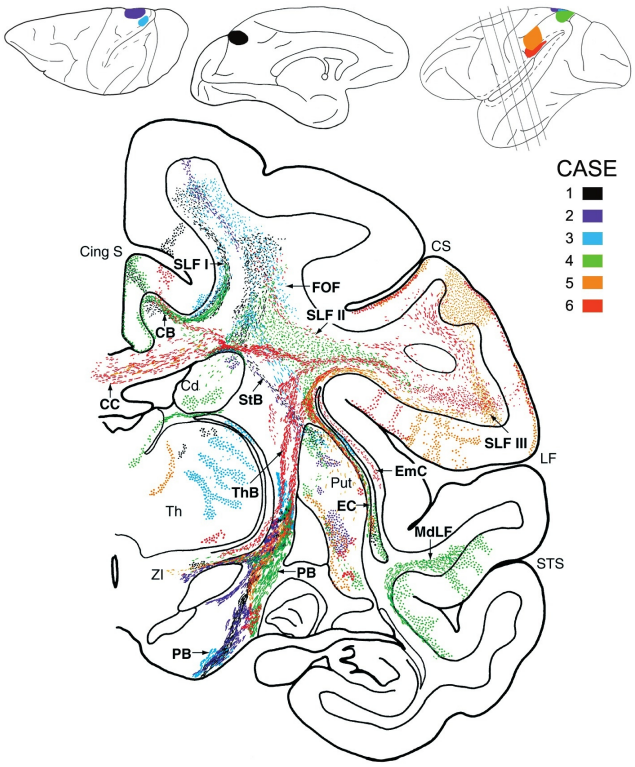

Figure 2: Composite diagram taken as example from Schmahmann and Pandya [30], page 139, Figure 6-13, slice 85, with the kind permission of the authors. In order to present the tract findings from 36 rhesus monkey brains combined into one picture, they draw the aggregated tracts onto a coronal slice from a healthy subject, called templated brain. The image illustrates white matter fiber pathways from six tracer injections. Each injection is color coded (cases 1 to 6) and the highlighted tracts are labeled with their respective names.

2.2 Methods for visualizing probabilistic tracts

Various approaches to visualizing probabilistic tractography data are described in literature. Such methods can be mainly categorized into groups, namely methods that provide a three-dimensional representation of probabilistic tractograms, slice-based techniques and glyph-based techniques.

2.2.1 Three-dimensional representations

Probabilistic tractograms are more appropriately described as a three-dimensional scalar field. Isosurfaces represent points of a fixed scalar value (isovalue) and can therefore give the user an initial impression of the data, as depicted in Figure 3a. However, isosurfaces also have several drawbacks.

First, there is the problem to choose a meaningful isovalue and second, the user has no visual feedback about the data besides the surface for the chosen isovalue. To mitigate the first problem, one may use nested, semi-transparent isosurfaces as depicted in Figure 3c. Many other methods may be used such as direct volume rendering of probabilistic tracts proposed by Kapri et al. [36], line construction algorithms such as *fODF-PROBA fibers* presented by Descoteaux et al. [10] or three-dimensional line integral convolution (LIC) proposed by Falk et al. [11]. A common problem of all of these three-dimensional representations is that it is hard to provide reasonable anatomical context. Either the representation occludes the context or the representation itself is partly occluded by the context hampering its interpretation. This holds even for the illustrative approach presented by Svetachov et al. [35].

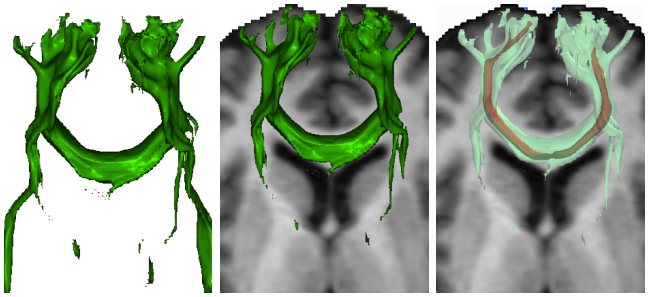

(a) Isosurface (b) Isosurface T1 (c) Nested isosurfaces

Figure 3: Different isosurfaces as examples for volumetric probabilistic tract representations. (a) Isosurface, (b) isosurface with axial T1 slice as anatomical context and (c) nested transparent isosurfaces with axial T1 slice as anatomical context

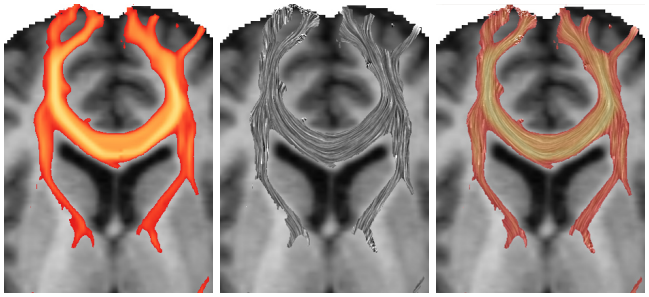

(a) Heat map (b) LIC (c) Colored LIC

Figure 4: Axial T1 slice with the same probabilistic tract but different overlays.

Topological visualization of probabilistic tracking as presented by Schultz et al. [31] may seem different from all these techniques. Still, as it uses nested 3D surfaces to depict the topology, it inherits the problems of all 3D and surface methods.

2.2.2 Slice-based Techniques

One reason why slice-based techniques are widely used in neuroscience is the fact that data from MRI scans is acquired and organized in slices. Slice-based techniques are generally used among neuroscientists since they provide a direct view of the original data. Another reason is that three-dimensional shapes may become overly complex very easily. However, the most crucial advantage is to provide a sufficient anatomical context. This is a difficult task for three-dimensional shapes but relatively easy for slice-based techniques. In practice, neuroscientists often use one or three slices representing the three standard orientations in sagittal, axial, or coronal view. These slices are just axis-aligned cutting-planes. Furthermore, deformed slices have been proposed by Anwander et al. [2, 32]. In this work we only apply axis-aligned slices. Hence, for obtaining reasonable volume representations, images need to be properly oriented in the underlying coordinate system.

Another (very basic) approach is to use color maps for rendering those parts of the probabilistic tractograms that are intersected by the cutting plane directly onto the cutting plane as depicted in Figure 4a. This visualization provides the presentation of probability distributions, whereas the underlying diffusion directions are not visible. More complex methods that are able to communicate the diffusion directions are the two-dimensional LIC, or techniques looking similiar to LIC as the one proposed by Calamante et al. [9]. It is generally applied to vector fields and uses only the directionality information as depicted in Figure 4b. A combination of LIC and color coding can convey both the diffusion direction and the probability value from the tractogram simultaneously, as shown in Figure 4c. However, the diffusion direction is not always easy to see and in particular regions of complex tract configurations, such as crossing tracts, would be very difficult to present.

2.2.3 Glyph-based Techniques

Tensor glyphs, such as ellipsoids, superquadrics [20] or tensor patches [7], provide a simple and direct way to represent local information in tensor data sets. Whereas their main purpose is to represent the full tensor information in a convenient and easily perceivable way, information that is not necessarily important to the user may become dominant, for example huge glyphs in areas not in the currently intended focus. Neuroscientists often are only interested in fiber bundles, which represent global connections in the brain, whereas glyphs are only used to study the local structure of the raw data. Nevertheless, our method has some similarities to glyph-based approaches:

- We represent the local direction of fiber tracts using stipples. But instead of overwhelming the user with additional information encoded in individual stipples (like for other glyphs [1, 12, 27]), the pattern of stipples provides information about the course and properties of fiber tracts. In addition, this has the advantage that stipples can be placed much closer than glyphs and, therefore, provide directional information at a much higher resolution.

- Placement of stipples, similarly to the placement of glyphs, plays an important role. While similar issues have recently been addressed for glyphs [21, 15], the underlying problem is somewhat different. Glyph-based approaches only work if every individual glyph is distinctly visible. In our approach, the reduction of each stipple to the important information renders this requirement unnecessary.

- The simplicity of individual stipples makes rendering fast and efficient and avoids the use of memory or processing power consuming approaches. This also holds for simple vector plots of the main diffusion direction. However, the arrows in conventional vector plots do not vary in density according to an additional scalar field [22] (in our case the probability). The reason behind keeping density in conventional vector plots constant is the aim to avoid misleading interpolation of the human visual system. The lengths of the arrows is simply perceived wrongly in this case. Additionally, vectors nearly parallel to the viewing direction, or, in our case, nearly orthogonal to the slice, become very small (nearly points) and can be easily missed. Our method counteracts this effect by using glyphs that all have the same area.

3 Methods

In order to produce a slice-based probabilistic rendering similar to the slices generated by Schmahmann and Pandya [30], we combine our tract rendering with boundary curves of the gray matter for anatomical context. In the following, we give a detailed description of the techniques we use for the anatomical context followed by a description of our illustrative probabilistic tract rendering. The procedures are identical for all slices and in particular for arbitrarily oriented slices. As mentioned above we provide only implementation details for axis-aligned slices.

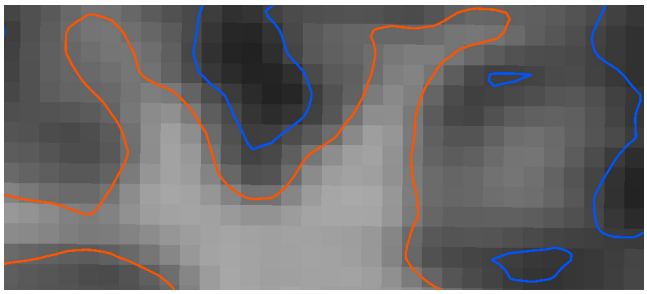

Figure 5: High resolution isolines for gray matter (blue) and white matter (orange) boundaries, derived from T1 image also used as non-interpolated background, to show the resolution difference.

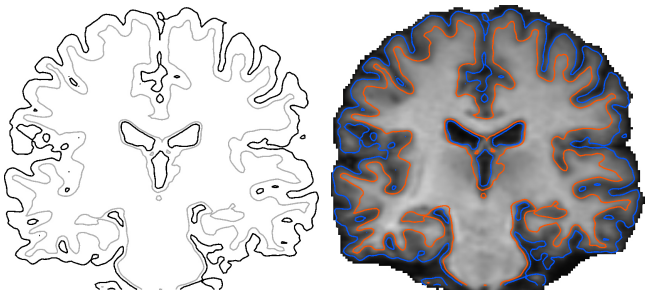

Figure 6: (a) Gray matter and white matter boundary curves derived from a T1 image. The T1 thresholds for gray matter and white matter were determined visually as depicted in (b). Prominent structures like the lateral ventricles or the superior frontal gyrus are easy to see and support orientation.

3.1 Anatomical context

Since anatomical context is a fundamental tool for neuroscientists we present this in two variants. First, we provide boundary lines indicating white matter and gray matter borders analog to those in the images from Schmahmann and Pandya. Secondly, these lines were combined with structural MRI data such as T1-weighted MR volume as shown in Figure 6. The user can interactively switch between these variants.

For boundary extraction, we use a 2D algorithm, also known as marching quads, which is closely related to the marching cubes algorithm presented by Lorensen et al. [24]. For each view, axial, sagittal and coronal, we define an implicitly represented regular two-dimensional grid consisting of quadrilateral cells. The T1 image is resampled for all vertices of this grid. For every edge of the grid we check whether interpolation of the T1 values along the edge crosses the selected isovalues for gray or white matter. For example, if an isovalue is between the values at the vertices building up the edge, this edge hits the isovalue. Once all those edges are determined, the isolines are generated from the crossing points on the edges. In order to provide high-quality isolines (see Figure 5) representing the usually used trilinear interpolant more accurately, the user may specify an arbitrary grid resolution. A higher resolution obviously leads to higher computation times for the isolines. With original T1 image resolution (1mm isotropic), the whole system is still very fast and interactive. For a grid with sixteen times the image resolution the computation is still performed within two seconds. If higher quality is needed, the system may slow down a bit. Straight-forward parallelization of the implementation could easily bring this below one second again. The thresholds can be visually adjusted within our tool, since they have to be determined for each subject. To ease this process we also provide also custom coloring of the isolines. For ideas how we could automate the determination of the thresholds we refer to Section 6.1.

3.2 Generating fiber stipples

As already mentioned, our visualization technique for probabilistic tracts is inspired by anatomical textbook drawings. For example the authors of *Fiber Pathways of the Brain*, Schmahmann and Pandya [30], use series of short lines and dots to represent the direction of fibers traced in microscopy images as depicted in Figure 2. We use line stipples similar to their traces to represent the main diffusion direction from the DTI data together with the topology of the scalar field from the probabilistic tracking (see Figure 1). This visualzation employs the metaphor of a slab showing only sections of fiber pathways lying in the slab. It thus mimics the short parts of the fibers in the tissue slabs traced using the microscope. In the following, we describe the generation of stipples.

We start with creating a two-dimensional regular grid on the given slice. By default the resolution of this grid is set to the native resolution of the datasets. Still, users may change the resolution of the grid in case they are interested in taking a closer look to a region of interest. However the resolution is set, this two-dimensional grid provides us with sample points for placing the lines stipples.

For each sample point and each tract, multiple line stipples may be drawn. Regions of high probability will result in a high density of line stipples, whereas regions with lower probability will exhibit a lower density. We linearly vary the density from ten stipples per cell down to zero in accordance with the probability. The placement of the line stipples for each sample point is achieved by generating jittered positions around the sample point inside its cell. We call this jittered position a center point for a line stipple. Looking up the probability and principal diffusion direction, that will determine the color and shape of a line stipple, is performed separately for each line stipple's center point by trilinear interpolation.

To achieve a discriminative coloring for the probabilistic tracts, we use the HSV color model [33] and uniformly distribute the tracts along the hue circle. Despite this preset, the user can choose to select a custom coloring for each tract. This is convenient to increase the contrast against the background (anatomical context) if necessary. Finally, the opacity of each line stipple is used to emphasize the tract's probability at the given center point.

The shape of each line stipple is determined by the principal diffusion direction at its center point. These directions are given as a vector field derived from the second-order tensor field. The vector field consists of the eigenvectors corresponding to the largest eigenvalues of the tensors. Since the center points are very unlikely to lie exactly on the grid vertices, we obtain the diffusion directions through component-wise interpolation. Unfortunately, this will produce interpolation artifacts as can be seen in Figure 7a. In oder to overcome those artifacts, we orient all eigenvectors into the same half space as suggested by Hotz et al. [16]. This is possible because the main diffusion direction is only defined up to its sign , meaning the eigenvectors $\mathbf{v}$ and $-\mathbf{v}$ are representing the same diffusion direction. The improvement is shown in Figure 7b.

Once a diffusion direction vector is computed, it is scaled to the size of a cell and projected onto the slice. Hence, a dot or a short line represents a diffusion direction perpendicular or nearly perpendicular to the slice, whereas a line with the length of the cell border represents a diffusion direction parallel to or *in* the slice. To further assist the user, in matching a line stipple's shape to the diffusion direction it represents, we provide a rendering of the slice grid which can be displayed on demand as depicted in Figure 8. In oder to achieve a smooth look, the line stipples' shape is rendered with round endings and a flat body as depicted in Figure 9a. The shape is determined by two points specifying the length of the stipple and a radius for its width. endings. The two points specifying the length

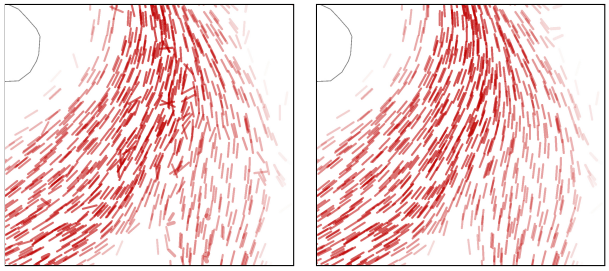

(a) (b)

Figure 7: Illustration of eigenvector interpolation artifacts (left) and stipples with corrected interpolation (right).

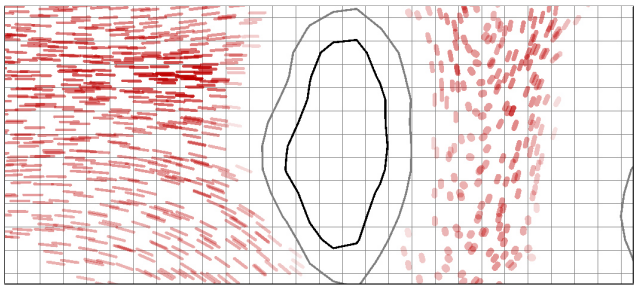

Figure 8: Optional slice grid giving the user a reference for the maximum length of line stipples. It can help to understand how parallel or orthogonal the represented direction is.

are given by the end points of the projected diffusion vector. As can be seen in Figure 9b, we vary the radius: It is increased if the line stipple's shape tends towards a dot and decreased if it tends towards a line. This produces a rendering where all stipples consume an equivalent area. This is desired because all diffusion directions are equally important. The area of a line stipple is given in Equation 1 and is set to fill a tenth of a cell area. This value is chosen to provide good results with the above mentioned ten stipples per cell. Solving Equation 1 for r, yields the radius needed to produce a shape with the desired radius.

$$A_{line\ stipple} = r^2\pi + 2r\overline{PQ} \tag{1}$$

In the renderings, the probability is represented by the opacity as well as by the density of the line stipples, whereas the diffusion direction is only represented by the shape of the stipples of equal area. Sometimes, it is convenient to focus only on regions of higher probability and fade out regions of lower probability. We therefore provide a threshold slider that lets the user hide all line stipples below the selected probability. Per default everything is shown.

Of course line stipples may overlap. However, compared to tensor glyphs, this does not cause a problem because the stipples are rendered in a semi-transparent fashion. Thus, overlapping stipples

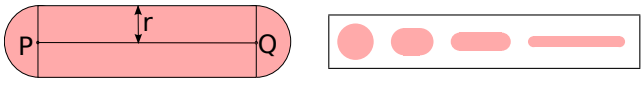

(a) (b)

Figure 9: (a) The structure of the line stipple is controlled by the two points P and Q and a radius r. The points P and Q are the endings of the diffusion vector projection onto the slice. The radius r is implicitly given by the area prescribed for the line stipple. (b) Different radii realizing area preserving line stipples.

can still be distinguished while the overlap provides a more natural look of the visualization as it resembles a manual drawing of stipples by a painter.

4 Data

To illustrate this novel method we applied it to MRI data of six healthy subjects. All structural data was acquired using Siemens 3-T Magnetom TRIO Scanners, located at the Max-Planck-Institute for Human Cognitive and Brain Sciences (Leipzig, Germany) and the Max-Planck-Institute for Neurological Research (Cologne, Germany). Diffusion data was measured along 60 gradient directions using a resolution of 1.72mm voxel size for up to $128 \times 128 \times 72$ voxels. Each gradient direction was measured three times to increase Signal-to-Noise ratio and therefore improve the robustness of tensor reconstruction and tractography. In addition a high-resolution T1-weighted image (1mm voxel size, $256 \times 256 \times 176$ voxels) was acquired for each subject to provide anatomical context. We use T1 images for that because they exhibit a high gray matter/white matter contrast [23] facilitating the extraction of the gray matter and white matter boundaries. After general preprocessing (e.g. motion correction) the diffusion data was resampled to 1mm voxel size, using the FSL software package [34]. Subsequently second order diffusion tensors and their corresponding major diffusion directions (principal eigenvectors) were derived on this interpolated data. Finally tractograms with similar seed regions for all subjects were created using the estimated diffusion tensors. For reference purposes we also computed a fractional anisotropy (FA) data set from the diffusion tensor image using the formula as given by Basser and Pierpaoli [4, 28]. In a second (optional) preprocessing step, the brains were extracted from their T1 images using FSL-BET from the FSL software package. In order to combine all data for visualization, all images of one subject must have the same resolution and have to be aligned to each other. This was realized by a linear registration of the T1 image into the diffusion space using FSL-FLIRT from the FSL software package.

If the diffusion-weighted image is not axis aligned we register all images to standard space MNI152 [25].

5 Results

We applied fiber stippling to the data, as described in Section 4, to show a single tract of a single subject in Figure 11 and multiple tracts of a single subject in Figure 10. It has also been tested with all other mentioned subjects and produced results of the same quality. In Figure 12, fiber stippling is applied to different subjects with different tracts to illustrate its robustness and flexibility.

As depicted in Figures 10, 11 and 12, the T1 boundary curves give a clear and precise context. Prominent features like the ventricular system and surface morphology (gyri, sulci) are well to discern. If even more detailed context is needed for example in regions deep inside the white matter, the plain T1 image or any other image can be easily combined with fiber stippling. As depicted in Figure 11b in the lower left, some times line stipples may break the boundary curves due to small local error in the registration process. Those artifacts appeared with linear as well as with nonlinear registration methods. However, this is not a problem of our method but of the preparation of the data. Such problems have to be solved by the domain experts themselves because a good registration is also important for nearly all other combinations of different measurements in research. Since the T1 intensities for the same tissue may vary between subjects and measurements, the thresholds for the boundary curves must be determined once for each image. In order to assist the user we provide an interactive slider to align the curves to an underlying T1 image.

Additionally, Figure 11f illustrates that fiber stippling is also able to effectively visualize the topology of a probabilistic tractogram.

In Figure 10 this is not prominent, because the focus is set to regions of higher probability values there. Since each tract uses just one color, even complex tract configurations like tract crossings, as depicted in Figure 10b, produce visually clear results as long as not too many tracts are used. The limitation of the number of tracts is a problem inherent in this type of illustration and is for example also present in Figure 2 where regions may occlude each other. Despite that, line stipples may also overlap and produce more opaque colored regions as if they were rendered solitary. However, this does not happen often and only in regions of high density where the probability is high anyway, so the representation of the topology is preserved. Furthermore, fiber stippling also reflects the directional information from the underlying tensor field, thus aiding understanding of tractography of a tract. With the jittered placement of line stipples, it is possible that some of the stipples form a short chain, producing the impression of a connected polyline. As we apply a random jittering, this happens only rarely and has no significant impact on the perceived directionality of the tract. Finally, the choice of a custom resolution enables the user to get a dense visualization (though only trilinearly interpolated) even for small regions and ease the comparison of regions in close-up views.

The performance of fiber stippling is primarily bounded by the resolution of the two-dimensional grid of each slice. Secondarily it is bounded by the number of probabilistic tracts used. The more tracts are used the more tracts must be checked for contributing line stipples in the stipple creation phase. An HP(R) Workstation Z600 with Intel(R) Xeon(R) CPU E5620, 32GB RAM and an Nvidia(R) Quadro FX 3800 graphics board with 1GB Memory served as test system. The time of rendering itself did never contribute noticeably to the overall runtime. Even with a mass of line stipples interaction (e.g. rotation) can be performed in real time. With native voxel size, anatomical context as well as line stipples need less than one second to be created. With four tracts, each contributing many line stipples, the whole process is done in about a second. If now the resolution is increased 16-fold, the performance decreases but will be below four seconds.

6 Conclusion

Fiber stippling, the illustrative technique for visualizing probabilistic tractograms presented in this paper, allows for a new interactive view on fiber pathways of the brain. The underlying metaphor of a slab showing only sections of pathways lying in the slab is intuitive and has already proven its usefulness in a widely used textbook that inspired the present paper. Although the use of transparency and stipple density is a direct consequence of the nature of the scalar fields representing the probabilistic tractograms, i.e. the decrease of the scalar (probability) from the seed point, the presented methods are directly applicable to scalar fields with other characteristics. Scalar fields representing masks can be the basis for fiber stippling visualization without any changes to the methods. Such masks can represent very different features. Examples range from fiber bundle volumes [13] to activations in functional MRI [6]. Fiber stippling can also be used to illustrate fuzzy fiber bundle descriptions like the one presented by Wassermann et al. [37].

We received very positive feedback from our collaborating neuroscientists. Actually, it was them who communicated a need for such a visualization in the first place. Fiber stippling is already in use in their daily work for discussing different tractography results and producing images for their research reports.

6.1 Future Work

For the future we plan to extend our work from DTI to HARDI (High Angular Resolution Diffusion Imaging) data. This will improve the illustration of fiber crossings where we only show the main diffusion direction at the moment. Compared to the textbook illustrations our method does not provide any labels yet. We are already working on an automatic labeling as an extension of the presented work. Additionally we want to ease the process of choosing the white matter and gray matter boundary thresholds with existing segmentation algorithms, like FSL-FAST from the FSL software package. Furthermore, we plan to improve the user interface of our method to allow an easy use in the OpenWalnut framework even for non-expert users. After publication of this article the described method will be freely available in OpenWalnut.

Acknowledgements

The authors wish to thank the OpenWalnut team, especially Sebastian Eichelbaum. OpenWalnut is an open source tool for multimodal medical and brain data visualization. This work was supported by the German Federal Ministry of Education and Research as part of the VisPME research collaboration (01IH08009F) as well as by the AiF (ZIM grant KF 2034701SS8). We also want to thank Jeremy D. Schmahmann and Deepak N. Pandya for their kind permission to use one of the pictures from their book *Fiber Pathways of the Brain*. Finally we also thank Christian Heine for his advice and assistance which improved this work.

References

[1] D. C. Alexander, G. J. Barker, and S. R. Arridge. Detection and modeling of non–gaussian apparent diffusion coefficient profiles in human brain data. *MRM*, pages 331–340, 2002.

[2] A. Anwander, R. Schurade, M. Hlawitschka, G. Scheuermann, T. Anderson, and T. R. Knösche. White matter imaging with virtual Klinger dissection. *NeuroImage*, 47(Supplement 1):S105 – S105, June 2009.

[3] A. Anwander, M. Tittgemeyer, D. von Cramon, A. Friederici, and T. Knösche. Connectivity-Based Parcellation of Broca's Area. *Cerebral Cortex*, 17(4):816–825, 2007.

[4] P. J. Basser and C. Pierpaoli. Microstructural and physiological features of tissues elucidated by quantitative-diffusion-tensor MRI. *Journal of Magnetic Resonance, Series B*, 111(3):209 – 219, 1996.

[5] T. Behrens, M. Woolrich, M. Jenkinson, H. Johansen-Berg, R. Nunes, S. Clare, P. Matthews, J. Brady, and S. Smith. Characterization and propagation of uncertainty in diffusion-weighted MR imaging. *MRM*, 50(5):1077–1088, 2003.

[6] J. Belliveau, D. Kennedy, R. McKinstry, B. Buchbinder, R. Weisskoff, M. Cohen, J. Vevea, T. Brady, and B. Rosen. Functional mapping of the human visual cortex by magnetic resonance imaging. *Science*, 254(5032):716–719, 1991.

[7] W. Benger, H. Bartsch, H.-C. Hege, H. Kitzler, A. Shumilina, and A. Werner. Visualizing Neuronal Structures in the Human Brain via Diffusion Tensor MRI. *Int. J. Neuroscience*, 116(4):461–514, 2006.

[8] J. I. Berman, S. Chung, P. Mukherjee, C. P. Hess, E. T. Han, and R. G. Henry. Probabilistic streamline q-ball tractography using the residual bootstrap. *NeuroImage*, 39(1):215–222, 2008.

[9] F. Calamante, J.-D. Tournier, R. M. Heidemann, A. Anwander, G. D. Jackson, and A. Connelly. Track density imaging (TDI): Validation of super resolution property. *NeuroImage*, 56(3):1259 – 1266, 2011.

[10] M. Descoteaux, R. Deriche, and A. Anwander. Deterministic and Probabilistic Q-ball Tractography: From Diffusion to Sharp Fiber Distribution. 2007.

[11] M. Falk and D. Weiskopf. Output-sensitive 3D line integral convolution. *IEEE TVCG*, 14(4):820 –834, Jul.-Aug. 2008.

[12] L. R. Frank. Characterization of anisotropy in high angular resolution diffusion-weighted MRI. *MRM*, 47:1083–1099, 2002.

[13] M. Goldau, A. Wiebel, M. Hlawitschka, G. Scheuermann, and M. Tittgemeyer. Visualizing DTI parameters on boundary surfaces of white matter fiber bundles. In J. Zhang, editor, *Proc. IASTED CGIM*, pages 53–61. ACTA Press, February 2011.

[14] P. Hagmann, L. Cammoun, X. Gigandet, S. Gerhard, P. E. Grant, V. Wedeen, R. Meuli, J.-P. Thiran, C. J. Honey, and O. Sporns. MR connectomics: Principles and challenges. *J. of Neuroscience Methods*, 194(1):34 – 45, 2010. Proceedings of the Workshop "Neuroanatomical Tracing and Systems Neuroscience: The State of the Art".

[15] M. Hlawitschka, G. Scheuermann, and B. Hamann. Interactive glyph placement for tensor fields. In *ISVC (1)*, pages 331–340, 2007.

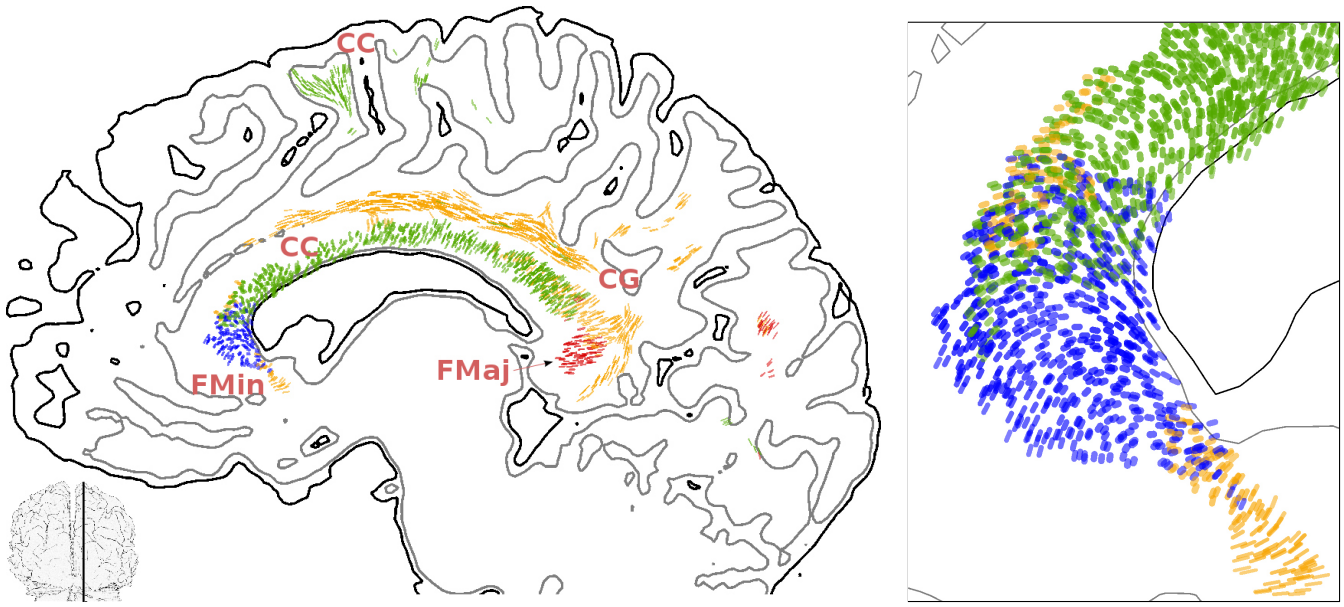

(a) (b)

Figure 10: (a) Sagittal section of the right hemisphere as depicted in the small overview in the lower left. Probability threshold is set to 0.5. Resolution is set to one fourth of the native resolution. Multiple probabilistic tractograms are drawn at once, labeled with the following abbreviations: (blue) FMin - forceps minor, (green) CC - corpus callosum, (red) FMaj - forceps major, (yellow) CG - cingulum bundle. (b) The close-up of the forceps minor shows tract overlappings as well as detailed direction information. Native voxel resolution is used. The probability threshold is set to 0.5.

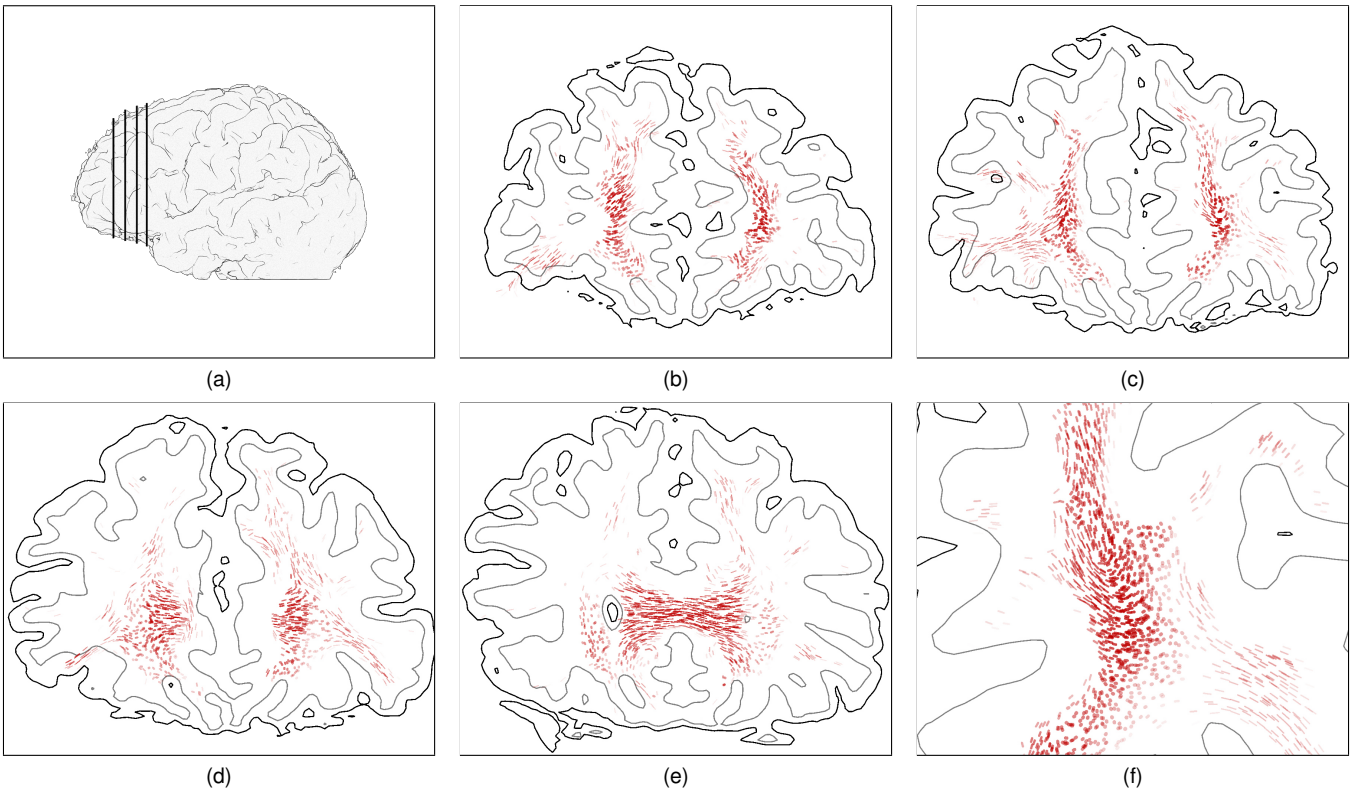

(a) (b) (c)

(d) (e) (f)

Figure 11: (a) Overview of four sections of the frontal lobe. Slices are depicted from left to right in images (b) to (e). (b)-(e) Different slice position of the same probabilistic tract, with no probability threshold and in a coarse resolution (one fourth of the native resolution). (f) Close-Up of left hemisphere of (c) showing detailed directional information in native resolution.

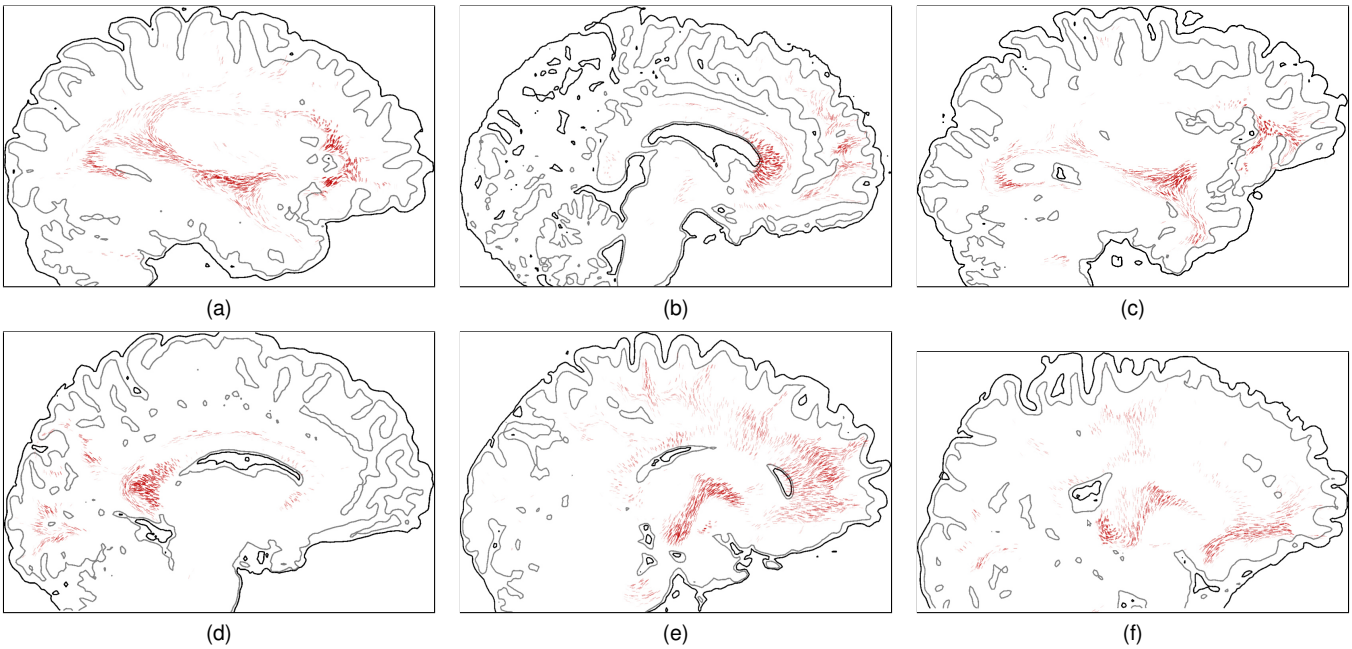

Figure 12: Fiber stipples applied to six different subjects all presenting a sagittal slice, with same probability threshold and slice resolution, but with a different probabilistic tract, different slice positions and subject specific thresholds for gray and white matter boundary curves.

[16] I. Hotz, J. Sreevalsan-Nair, H. Hagen, and B. Hamann. Tensor field reconstruction based on eigenvector and eigenvalue interpolation. In *Scientific Visualization: Advanced Concepts*, volume 1 of *Dagstuhl Follow-Ups*, pages 110–123. Schloss Dagstuhl, 2010.

[17] W.-K. Jeong, P. T. Fletcher, R. Tao, and R. Whitaker. Interactive visualization of volumetric white matter connectivity in DT-MRI using a parallel-hardware hamilton-jacobi solver. *IEEE TVCG*.

[18] H. Johansen-Berg and T. E. J. Behrens. *Diffusion MRI: From Quantitative Measurement to In Vivo Neuroanatomy*. Academic Press, 2009.

[19] H. Johansen-Berg and M. F. Rushworth. Using diffusion imaging to study human connectional anatomy. *Annual Review of Neuroscience*, 32(1):75–94, 2009. PMID: 19400718.

[20] G. Kindlmann. Superquadric tensor glyphs. In *Proc. VisSym 2004*, pages 147–154, May 2004.

[21] G. Kindlmann and C.-F. Westin. Diffusion tensor visualization with glyph packing. *IEEE TVCG*, 12(5):1329–1335, Sep-Oct 2006.

[22] Kitware Inc. *VTK User's Guide*. Kitware Inc., March 2006.

[23] M. G. Linguraru, T. Vercauteren, M. Reyes Aguirre, M. A. González Ballester, and N. Ayache. Segmentation propagation from deformable atlases for brain mapping and analysis. *Brain Research Journal*, 1(4):269–287, 2007.

[24] W. E. Lorensen and H. E. Cline. Marching cubes: A high resolution 3D surface construction algorithm. In *SIGGRAPH '87: Proceedings of the 14th annual conference on Computer graphics and interactive techniques*, pages 163–169, New York, NY, USA, 1987. ACM.

[25] J. Mazziotta, A. Toga, A. Evans, P. Fox, J. Lancaster, K. Zilles, R. Woods, T. Paus, G. Simpson, B. Pike, C. Holmes, L. Collins, P. Thompson, D. MacDonald, M. Iacoboni, T. Schormann, K. Amunts, N. Palomero-Gallagher, S. Geyer, L. Parsons, K. Narr, N. Kabani, G. Le Goualher, D. Boomsma, T. Cannon, R. Kawashima, and B. Mazoyer. A probabilistic atlas and reference system for the human brain: International Consortium for Brain Mapping (ICBM). *Philosophical transactions of the Royal Society of London. Series B, Biological sciences*, 356(1412):1293–1322, Aug. 2001.

[26] S. Mori and P. C. M. van Zijl. Fiber Tracking: Principles and Strategies – A Technical Review. *NMR in Biomed.*, 15(7-8):468–480, 2002.

[27] E. Özarslan and T. H. Mareci. Generalized diffusion tensor imaging and analytical relationships between diffusion tensor imaging and high angular resolution diffusion imaging. *MRM*, 50:955–965, 2003.

[28] C. Pierpaoli and P. J. Basser. Toward a quantitative assessment of diffusion anisotropy. *MRM*, 36(6):893–906, 1996.

[29] M. Reisert, I. Mader, C. Anastasopoulos, M. Weigel, S. Schnell, and V. Kiselev. Global fiber reconstruction becomes practical. *NeuroImage*, 54(2):955 – 962, 2011.

[30] J. D. Schmahmann and D. N. Pandya. *Fiber Pathways of the Brain*. Oxford University Press, 2006.

[31] T. Schultz, H. Theisel, and H.-P. Seidel. Topological Visualization of Brain Diffusion MRI Data. *IEEE TVCG*, 13:1496–1503, 2007.

[32] R. Schurade, M. Hlawitschka, B. Hamann, G. Scheuermann, T. R. Knösche, and A. Anwander. Visualizing white matter fiber tracts with optimally fitted curved dissection surfaces. In *VCBM 2010 Eurographics Workshop on Visual Computing for Biology and Medicine*, pages 41–48. Eurographics Association, July 2010.

[33] A. R. Smith. Color gamut transform pairs. In *Proceedings of the 5th annual conference on computer graphics and interactive techniques*, SIGGRAPH '78, pages 12–19, New York, NY, USA, 1978. ACM.

[34] S. Smith, M. Jenkinson, M. Woolrich, C. Beckmann, T. Behrens, H. Johansen-Berg, P. Bannister, M. D. Luca, I. Drobnjak, D. Flitney, R. Niazy, J. Saunders, J. Vickers, Y. Zhang, N. D. Stefano, J. Brady, and P. Matthews. Advances in functional and structural MR image analysis and implementation as FSL. *NeuroImage*, 23(S1):208–219, 2004.

[35] P. Svetachov, M. H. Everts, and T. Isenberg. DTI in Context: Illustrating Brain Fiber Tracts In Situ. *CGF*, 29(3):1024–1032, Jun 2010.

[36] A. von Kapri, T. Rick, S. Caspers, S. B. Eickhoff, K. Zilles, and T. Kuhlen. Evaluating a visualization of uncertainty in probabilistic tractography. In K. H. Wong and M. I. Miga, editors, *Proc. SPIE*, volume 7625, page 762534. SPIE, 2010.

[37] D. Wassermann, L. Bloy, E. Kanterakis, R. Verma, and R. Deriche. Unsupervised white matter fiber clustering and tract probability map generation: Applications of a gaussian process framework for white matter fibers. *NeuroImage*, 2010.